Enhanced cell killing and apoptosis of oral squamous cell carcinoma cells with ultrasound in combination with cetuximab coated albumin microbubbles

Abstract

Targeted microbubbles has the potential to be used for ultrasound (US) therapy and diagnosis of various cancers. In the present study, US was irradiated to oral squamous cell carcinoma cells (HSC-2) in the presence of cetuximab coated albumin microbubbles (CCAM). Cell killing rate with ultrasound treatment at 0.9W/cm^2 and 1.0W/cm^2 in the presence of CCAM was greater compared to non-targeted albumin microbubbles ($p<0.05$). On the other hand, selective cell killing was not observed in human myelomonocytic lymphoma cell line (U937) that had no affinity to cetuximab. Furthermore, US irradiation in the presence of CCAM showed a five-fold increase of cell apoptotic rate for HSC-2 cells (21.0±3.8%) as compared to U937 cells (4.0±0.8%). Time-signal intensity curve in a tissue phantom demonstrated clear visualization of CCAM with conventional US imaging device. Our experiment verifies the hypothesis that CCAM was selective to HSC-2 cells and may be applied as a novel therapeutic/diagnostic microbubble for oral squamous cell carcinoma.

Keywords: ultrasound, cetuximab, albumin, targeted microbubble, oral squamous cell carcinoma, apoptosis, ultrasound imaging

To link to this article: http://www.tandfonline.com/doi/full/10.1080/1061186X.2017.1367005

Introduction

Head and neck cancer is the sixth most common cancer worldwide [1]. They include cancers of the larynx, throat, lips, and salivary glands. Oral squamous cell carcinoma (OSCC), originating in the mouth and lips makes approximately 90% of all oropharyngeal malignancies [2]. Although smoking and excessive alcohol consumption are prominent oral cancer risk factors, human papillomavirus infection and population aging have greatly contributed to the increased cancer incidents in recent years [3]. Efforts have been made on various aspects for OSCC, including detection techniques, radical removal of the malignant tissue, and mechanisms involved in cancer initiation and progression. In addition, several strategies have been proposed to induce tumour sensitivity to radiation or anticancer drugs [4]. In spite of these recent advances, OSCC still is among the tumour types with a poor prognosis [5]. Thus, more effective diagnostic and therapeutic strategies are urgently needed to combat this deadly disease.

Recently, a novel ultrasound/microbubble-mediated technique has been explored as a potential drug carrier for effective accumulation within various tumour tissues [6-10]. Furthermore, combining tumour targeting, imaging and therapeutic function into a single microbubble (MB) has generated great attention because of its ability to simultaneously diagnosis and treat cancers, to be specific; by means of contrast echography and therapeutic ultrasound. Microbubble shells made of albumin are especially attractive for its multiple beneficial features such as, non-antigenicity, biodegradability, easy preparation, reproducibility, and non-toxicity. Microbubble agents have previously been developed for ultrasound contrast imaging which contains an air core and stabilized by albumin (Albunex®). Currently available bubble contrast agent, Optison® (GE Healthcare Systems, PA, USA) has a perfluoropropane gas core with an albumin shell. Additionally, albumin MBs have a

potential of becoming a versatile platform for many types of molecular targeted therapy agents bounded by ionic interaction, or dispersement in the albumin particle matrix [11, 12]. Various biomolecules such as antibodies can be conjugated onto the surface of albumin MBs to offer active targeted diagnosis or treatment of cancers. These biomolecules can be designed to interfere with a specific molecular target or signaling pathway that may play a key role in tumour growth or progression and induce apoptosis. Cetuximab (Erbitux®) is a chimeric human/murine monoclonal antibody in the immunoglobulin (Ig) G1 class that specifically targets the human epidermal growth factor receptor (EGFR) with higher affinity than the natural ligands, transforming growth factor-α and epidermal growth factor [13, 14]. Preclinical studies have demonstrated anti-tumour activity of cetuximab such as G0/G1 cell-cycle arrest, induction of apoptosis, inhibition of DNA repair, inhibition of angiogenesis, inhibition of tumour cell motility, and metastasis [15]. It is currently indicated for the treatment of locally advanced squamous cell carcinoma of the head and neck in combination with radiation therapy and for treatment of recurrent or metastatic carcinoma [16].

The mechanism of cell damage to cancer cells by ultrasound is not clear. However, some researchers have hypothesized that oscillating MBs during ultrasound exposure attribute to cell killing [17, 18]. Ultrasound induces cavitation or oscillation of MBs thus generating violent fluid flow surrounding the bubble. This phenomenon causes shear stress on the cell membrane leading to cell damage [19]. If this hypothesis proves to be true, it is safe to say that the less the distance from cavitation occurrence and cell membrane would induce greater mechanical force to damage or kill cancer cells. Feril et al. [20] have demonstrated enhanced ultrasound induced apoptosis in the presence of ultrasound contrast agent MBs. It was suggested that MBs have the potential to be adjuncts in cancer therapy. Custom made MB that has the function to specially adhere to specific cancer cells such as OSCC could lead to an ideal theragnostic agent.

In order to obtain the above objective in the most effective means, we coated an ultrasound contrast agent albumin MB with cetuximab which can be used for specific targeting of the EGFR expressed on the surfaces of OSCC. In the present report, the immediate increase in the selective tumour cell killing and apoptosis by therapeutic ultrasound was compared between EGFR expressed and non-EGFR expressed tumour cells *in vitro*. We also evaluated if this contrast agent can be visualized with a conventional US imaging device.

Methods & Materials

Preparation of microbubbles

The MBs used in this study had an albumin outer shell, each entrapping perfluoropropane gas. They were prepared by the following method at our laboratory, according to the established favorable production conditions. In brief, a 700 µl sterile solution of 0.25 % human serum albumin (fraction V, purity 96%; Aventis Behring L.L.C., IL, USA) in phosphate-buffered saline (PBS; 140 mM NaCl, 2.7 mM KCl, 10 mM Na_2HPO_4 and 1.8 mM KH_2 PO_4, pH 7.4; Cosmo Bio Co., Tokyo, Japan) was added in a air filled 2 ml plastic tube. After air tight sealing, the air within the container was replaced with perfluoro-propane (C3F8; Takachiho Chemical Industrial Co, Tokyo, Japan) gas using a 23-gauge needle inserted through a customized 3D printer manufactured cap. The container tubes were then placed into a high speed shaking tissue homogenizer device (Precellys Evolution, Bertin Instruments, France), they were shaken at high speeds under the following conditions: 6500 rpm, 6 x 10s duration, 20 second pause between each shaking phase. The MBs were preserved in a 4 °C condition until use.

Characterization of microbubble

In order to measure the physical properties of albumin MBs, a light scattering measurement system ELSZ - 2000ZS (Otsuka Electronics Co., Osaka, Japan) was used. The measurement principle is dynamic light scattering (DLS) which observes temporal change or fluctuation of scattered light from Brownian moving particles which estimates the overall size distribution of bubbles. The measurement range of the device was 0.6 nm to 10 um. All measurements were carried out at room temperature by adding 1 mL of the sample to the glass cell. Repeated measurements were carried out 3 times for each sample, and averaged to determine particle diameter. The size distribution of the albumin MB is depicted by the curve shown in Fig. 1. The mean size of albumin MBs used throughout the experiments was 1278 ± 54.49 nm and MB concentration approximately 5×10^8 /mL.

Cell culture

Oral squamous carcinoma cell line HSC-2 were purchased from JCRB (Japanese Collection of Research Bioresources) cell bank and cultured in Minimum Essential Medium (MEM; Nacalai tesque, Kyoto, Osaka, Japan) with 10% Fetal Bovine Serum (Invitrogen Co., Tokyo, Japan) and was maintained at 37.0℃ in humidified air with 5% CO_2. HSC-2 cells collected by trypsin–EDTA (Gibco, NY, USA) were washed and maintained in fresh medium immediately before each sonication experiment. Similarly, human myelomonocytic lymphoma cell line U937 (~~Japanese Collection of Research Bioresources~~ JCRB Cell Bank) was cultured in Roswell Park Memorial Institute medium ~~RPMI 1640~~ (RPMI 1640; Nacalai tesque, Kyoto, Japan) supplemented with 10% Fetal Bovine Serum (Sigma-Aldrich, MO, USA) , maintained at 37.0 °C in humidified air with 5% CO_2. On the day of experiment, cells were collected and centrifuged at 100g for 5 min. Both cell lines were free of viral pathogens with initial viability of more than 99% were used for the actual experiments.

Preparation of antibody

Cetuximab is a human-mouse chimeric monoclonal antibody belonging to the IgG1 family. This treatment is approved by the FDA for metastatic colorectal cancer that express EGFR, such as head and neck cancer. Cetuximab was purchased from Merck-Serano (Erbitux®, Geneva, Switzerland) and was mixed in the MB included reagent at concentrations of 125, 250, 375 μg/mL immediately prior to ultrasonic irradiation to the cells. The antibody and microbubble was bond by electrostatic interactions.

Cell viability measurement

The number of viable HSC-2 cells and U937 were measured immediately after all treatments using a trypan blue dye exclusion method. The cell suspensions were mixed with an equal volume of trypan blue stain (0.4%). We considered that both dead and dying cells stained with trypan blue as nonviable, and that the cells not stained with trypan blue as viable. The number of viable cells was counted with a fully automated cell counter (Automated cell counter TC20, BioRad, CA, USA) that uses multi-focal plane imaging analysis for live/dead cells. The survival rate of treated cells was calculated as the ratio of the number of surviving cells to the number of control non-treated surviving cells. Each irradiation and drug condition treated cell survival rate data consisted of at least four repeated samples (n = 4).

Ultrasound apparatus and irradiation protocol

Both cancer cells lines HSC-2 or U937 were sonicated in culture multi-wells. The ultrasound condition and microbubble concentration was based on experiments previous described [21]. The ultrasound exposure system (Fig 2) consists of 4 independent ultrasound generators (KTAC-4000, NepaGene, Chiba, Japan) and 4 unfocused-single-20mm diameter ultrasound transducers (KP-S20, NepaGene, Chiba, Japan). The 24 well cell culture plate

(SARSTEDT Lumox® multiwell 24, Nümbrecht, Germany) was placed on the acoustic radiation surface of ultrasound transducers via ultrasound transmission gel (Aquasonic 100, Parker lab, NJ, USA). The plate bottom consists of a 50 μm thick polystyrene acoustically transparent film described elsewhere [22] for sufficient ultrasound exposure. The 4 ultrasound transducers were driven by the 4 different ultrasound generators at the driving frequency of 1.0 MHz, the burst rate of 10 Hz and the duty ratio of 50%, and the ultrasound were generated simultaneously from the ultrasound transducers. The US generator can operate at fixed frequency in the continuous wave mode or in the pulsed wave mode. Ultrasound energy with 3 acoustic intensities Ispta (spatial peak temporal average) of 0.8, 0.9 and 1.0 W/cm^2 (150 kPa, 160 kPa, 170 kPa , respectively) were exposed simultaneously to the 4 wells of the 24 well cell culture plate for 15 second. The 4 wells were sonicated in the same acoustic conditions by placing each of the multiple plates so that the wells of interest were perfectly centered above the 4 transducers. Thermal change near the transducer were monitored by a digital meter connected to one of the four transducers which showed reading below 25 °C at all times.

HSC-2 cells were re-suspended in fresh MEM medium with 10% FBS at a final concentration of 1×10^6 cells/mL. 2 mL of cell suspension were added to the each well of 24 well cell culture plate. 250 μL of cetuximab molecular targeted microbubble was added to the 2 mL of cell suspension in each well. After 5 minutes, ultrasound was exposed to the HSC-2 cells and MBs. US irradiation experiment consisted of four groups: non-treated control, ultrasound alone, non-targeted albumin MB combined with ultrasound, cetuximab molecular targeted MB combined with ultrasound. After ultrasound irradiation treatment, HSC-2 cells were collected immediately from each well of the 24 well plates. Trypan blue dye exclusion test was performed immediately for measurement of cell survival rate. The cancer cell line U937 was similarly prepared and treated in the same ultrasound conditions and groups as the

HSC-2 cells. The ratio of the total number of microbubbles within the medium and cells was approximately 63 to 1.

Apoptosis measurement

The apoptotic events of HSC-2 and U937 cancer cells were measure by the Tali® Image-Based Cytometer (Life Technologies Japan, Tokyo, Japan) which is a 3-channel (bright field, green fluorescence, red fluorescence). The device captures up to 20 microscopic slide images per sample and automatically analyses the images with digital image based cell counting and fluorescence detection algorithms. Briefly, after 6-h incubation in humidified air with 5 % CO2 at 37 °C, the cancer cells were subjected to trypsinization, a 100 μL aliquot of cells (1×10^6) from each sample was centrifuged at 100g and resuspended in 100 μL apoptosis buffer (50 mM HEPES, 700 mM NaCl, 12.5 mM $CaCl_2$, pH 7.4) added to 5 μL Annexin V (5%; conjugated with Alexa Fluor® 488, Thermo Fisher Scientific, MA, USA) and incubated at room temperature in the dark for 20 min. Then, the samples were centrifuged (100g) and resuspended again in 100 μL of the same buffer and added with 1 μL Propidium Iodide (1% PI; Tali® Viability Kit; Life Technologies Japan, Tokyo, Japan) at room temperature in the dark for 1–5 min and analysed by Tali® Image-Based Cytometer. Apoptotic cells showed green fluorescence, late apoptotic cells showed red and green fluorescence, and live cells showed low or no fluorescence. Apoptosis was calculated as the percentage of apoptotic cells/the number of total cells in each group. Each measurement was repeated three times independently.

Fluorescence microscopy

In order to visualize the existence of cetuximab on the surface of targeted MBs, fluorescently labelled antibody method was used. Readilink® antibody labelling kit

specifically fluorescence tags cetuximab. Briefly, solution of 1 mg/ml concentration antibody labelling fluorescence was suspended with the targeted antibody in PBS. Antibody solution of 50µl was added to 5µL reaction buffer. After mixing sufficiently several times by pipetting, the antibody solution total amount (55µl) was added to one vial of ReadiLink dye (BioRad Laboratory, CA, USA). It was incubated for 60 minutes at room temperature. Fluorescent block buffer (Quench buffer) was added to 5µl to the reaction mixture solution and incubated at room temperature for 10 minutes. Molecular Probes® Texas Red Albumin was adjusted to 3% of total concentration of albumin for visualizing albumin MBs. Fluorescent labeled antibodies, albumin and cells were observed with a bright field and multichannel fluorescence integrated inverted microscope equipped with a digital camera, and a touch-screen interface (ZOE ™ Fluorescent Cell Imager Bio-Rad Laboratories, CA, USA). Green LED channel was: excitation, 480/17 nm; emission: 517/23 nm and red LED channel was: excitation, 556/20 nm; emission, 615/61 nm. Magnification was 20 times for all observations.

Bright field cell/bubble analysis

Five investigators with medical background were randomly selected from our department and were asked to count the number of MBs in contact with cell surface in each of the microscopic bright field cell photos provided. Cell images were randomly deprived from microscopic images obtained in the course of the experiments. A total of 40 condition blinded photos of HSC-2 cell which half included targeted MBs and the remaining non-targeted MBs. The microscope magnification rate was 20 times. The counted results were later statistically analyzed.

Ultrasound imaging process

The blood vessel-mimicking flow model system for ultrasound imaging evaluation consisted of a 3 mm diameter and 15 cm in length lumen in a commercially available tissue ultrasound phantom (6x15x8cm,VP-3 ATS laboratories, CT, USA). The albumin MB solution described previously (0.25 % human serum albumin) was diluted 20 times by PBS and was injected through the vessel at a constant speed of 0.3 ml/min using a syringe injection pump (YSP-201, YMC Ltd, Kyoto, Japan). Microbubble imaging evaluation was performed with a conventional clinical ultrasound machine (Logiq 9; GE Healthcare, WI, USA). A ML6-15 liner array transducer probe with transmission frequency of 6 – 15 MHz for both standard and contrast-enhanced was used. The ultrasound probe was placed and fixed on the top surface of flow phantom with ultrasound gel (AQUASONIC® 100, Parker labs, NJ, USA) between the probe and phantom. Enhanced signal intensity as a function of time in the lumen of the flow vessel was obtained in the contrast enhance mode.

Statistics

Measurement data were displayed as mean ± standard deviation (SD). Data was analyzed using unpaired t-test including Welch's correction. The statistical significant differences between various groups were analyzed using SPSS software (IBM, NY, USA). The probability value of $p<0.05$ was considered statistically significant.

Results

Drug toxicity evaluation

To investigate the immediate cell toxicity of cetuximab alone to HSC-2 and U937 cell lines, cetuximab was administered at various concentrations and assessed by trypan blue staining cell viability assay. Cell survival rate of HSC-2 cells at cetuximab concentrations 125μg/ml, 250μg/ml, 375μg/ml were 99.6±4.9%, 98.0±4.3% and 95.4±1.8%, respectively (Fig. 3A). Similarly, cell survival rate of U937 cells with cetuximab concentrations 125μg/ml, 250μg/ml, 375μg/ml were 99.6±3.7%, 94.6±8.4% and 93.1±4.9%, respectively (Fig. 3B). Immediate toxicity of cetuximab at these specific concentrations was not observed in both HSC-2 and U937 cell lines.

Effect of ultrasound alone

The effect of ultrasound alone at various irradiation intensities to HSC-2 cells and U937 cells are shown in Fig. 4. Cell survival rate of HSC-2 cells after ultrasound treatment at 0.8W/cm^2, 0.9W/cm^2, 1.0 W/cm^2 were 96.5±5.4%, 89.5±9.2% and 76.1±11.7%, respectively. There were no statistically significant differences ($p<0.05$) compared to the control group, but the cell survival rate tended to decrease with increased ultrasound irradiation intensities. Similar tendency was observed for U937 cells. Cell survival rate immediately after treatment by ultrasound alone at 0.8W/cm^2, 0.9W/cm^2, 1.0W/cm^2 were 90.1±4.5%, 78.1±2.8% and 79.8±4.6%, respectively.

Cell killing by targeted microbubbles

Enhanced cell-killing effect of ultrasound in the presence of MBs both in HSC-2 and U937 cells are shown in Fig.4. In order to investigate whether ultrasound in the presence of MBs

could specifically kill HSC-2 cells, we compared the cell killing effect of targeted/non-targeted MBs versus ultrasound alone (without MBs) to HSC-2 cells under various ultrasound intensities (Fig. 4A). There was significant difference of cell survival between targeted MBs versus ultrasound alone treated cells at 0.9W/cm^2 and 1.0W/cm^2. No significant difference of cell killing was observed between targeted MBs and ultrasound alone treated cell at 0.8W/cm^2. Cell survival rate with ultrasound treatment at intensities 0.8W/cm^2, 0.9W/cm^2 and 1.0W/cm^2 in the presence of targeted MBs were 87.2±5.2%, 69.0±7.7%, 60.8±6.7%, respectively. In contrast, cells treated with ultrasound in the presence of non-targeted MBs, showed no significant difference of cell survival compared to ultrasound alone treated cells at all ultrasound intensities. To determine if the above results were specific to EGFR positive cells, the same treatment to U937 cancer cells which have no EGFR receptors to the cell membrane was performed. Results revealed no difference of cell killing both for targeted and non-targeted MBs at all ultrasound intensities. Cell survival rate with ultrasound treatment at intensities 0.8W/cm^2, 0.9W/cm^2 and 1.0W/cm^2 in the presence of non-targeted MBs were 73.7±10.6%, 75.4±3.8% and 67.2±9.3%, respectively. Similarly, U937 cells treated with ultrasound at all intensities in the presence of targeted MBs also revealed no significant difference of cell killing as compared with ultrasound alone treatment.

Induction of apoptosis

Fig 5 shows the ~~apoptosis~~ rate of apoptotic cells (total of the early and late stages) of both HSC-2 and U937 cells under the presence of MBs and/or ultrasound treatment. Comparison of the number of apoptotic cells between HSC-2 and U937 cells resulted in no significant difference in the controls, US alone irradiated, and non-targeted MBs plus US. Whereas, in the presence of targeted-MBs plus US, there was a five-fold increase of apoptotic cells for

HSC-2 as compared to U937 cells. Apoptosis induced by ultrasound in the presence of targeted MB was 4.0±0.8% for U937 cells and 21.0±3.8% for HSC-2 cells.

Microbubble characterization

Images of fluorescent labeled Cetuximab-MBs were captured by multichannel fluorescence microscopy and shown in Fig. 6. Albumin MBs appeared as small dark spots in bright field images, some adhering to the surface of cancer cells (Fig. 6A). Texas Red-stained albumin MBs were observed on the MBs and adhered or located in the vicinity of the HSC-2 cells (Fig. 6 B). Moreover, in comparison to the uniform red color of cell image in red field, Readilink® green dye labeled anti-EGFR-antibody (Cetuximab) could also be observed as a bright green fluorescence near the cell membrane (Fig. 6 C). After merging the images of red and green fluorescence images, the location of MBs (red) and the anti-EGFR-antibody zone (green) overlapped (Fig. 6 D), indicated they were same MBs.

The blinded images of the cells were examined by the investigators and the number of targeted/non-targeted MBs adhering to HSC-2 cells were counted. The average number of targeted MBs in contact with the cell membrane surface was 70.1 ± 1.2 per image whereas the number of non-targeted MBs was 24.5± 0.7 per image (Fig. 7). There was statistical difference between these two groups ($p<0.05$).

Ultrasound imaging in a flow phantom was carried out in order to examine the echogenicity of the albumin MBs. Fig. 8A shows ultrasound images before injection of albumin MBs. Flow vessel could be characterized within normal tissue phantom by standard ultrasound imaging. No enhancement was observed in the flow vessels in the contrast-imaging mode. Whereas, immediately after MB injection, MBs were detected as acoustic signals in standard mode while enhancement was obtained within the flow vessel lumen by contrast imaging (Fig. 8B). The region of interest (ROI) was created within the flow vessel lumen. Time signal

intensity curve, in the lumen of the flow vessel, increased from baseline to peak intensity in approximately 40 seconds. The targeted and non-targeted albumin MBs could be clearly visualized by ultrasound imaging (Fig. 8C, D). Signal to noise ratio (SNR) baseline intensity before injection of albumin MBs was ~~-50.1± 0.1 dB~~ -58.6± 0.2 dB (Fig. 8 A) and enhanced intensity after injection of albumin MBs was ~~-42.5± 2.4~~ -40.1± 0.5 dB (Fig. 8 B). Similarly, baseline intensity before injection was -58.3± 0.2 dB and enhanced intensity after injection of targeted albumin MBs was -42.8± 0.5 dB. The mechanical index (MI) was ~~0.11~~ 0.12(frequency 5-16 MHz). Contrast to tissue ratio (CTR) was 15.3 dB for albumin MBs and 15.5 dB for targeted albumin MBs.

Discussion

There has recently been great expectation of using albumin as a drug carrier [23]. Albumin is the most abundant protein in the plasma and non-toxic with no immunogenicity. Some of the research work recently reviewed by Liu et al. [24] have referred albumin as an excellent candidate for many pharmaceuticals. The amino acid residues on albumin can be readily linked with therapeutic drugs, imaging reporters and targeting molecules through chemical conjugation. The enhanced permeability and retention (EPR) effect of albumin is also a unique advantage for carrying anticancer drugs to specific tumour regions. Albumin is a natural carrier of hydrophobic molecules with favorable, non-covalent binding characteristics thus various drugs can be incorporated into the particle matrix because of the different drug binding sites present in the albumin molecule. Albumin has also been used for ultrasound contrast agents for some time. One of the early commercial ultrasound contrast agent was an air-filled albumin microspheres prepared from sonicated 5% human serum albumin. The 2nd generation albumin ultrasound contrast agent, contained perflutren as a gas core [25]. These MBs have been shown in the clinical situation to be a useful echocardiographic contrast agent on coronary blood flow, left ventricular function, and systemic hemodynamics. Recently, phospholipid-stabilized MBs of sulfur hexafluoride gas or perfluorobutane gas have been introduced for diagnostic imaging of the liver or breast. These contrast agent MBs typically have a mean diameter ranging from 1 to 10 μm. In the present study, the albumin MB average diameter was approximately 1 μm that is relatively small compared to previous albumin based ultrasound contrast agents. Bubbles smaller than 1 μm, frequently termed as nanobubbles have recently attracted much attention from the fact that they can cross the vascular wall and reach tumour cells [26]. Although a portion of our bubbles were in the sub micron size range, our echography evaluations under physiologically relevant flow conditions suggests that the echogenic signals are sufficient for enhancing small blood vessels and

differentiating tumours with normal tissues. However, further *in vivo* animal studies are required to assess the feasibility of using this specific MB before final application to the clinical stage.

Recent advance in investigating the molecular basis of cancer have produced a whole new generation of promising therapies designed to target specific cell receptors that promote tumour growth and survival. One of the first novel molecular targeted therapies was inhibiting activation of the epidermal growth factor receptor (EGFR). Ligand binding induces receptors to dimerise and activate the intracellular kinase domain present on each receptor, resulting in phosphorylation of tyrosine residues on each member of the receptor pair. The EGFR signal network then stimulates multiple cellular responses including proliferation, survival, angiogenesis and metastasis. Cetuximab specifically binds to the EGFR with high affinity, preventing the ligand from interacting with the receptor, thus blocking growth factors from accessing the receptor and EGFR simulation signal transduction pathways [27]. Previous studies have evaluated the possibility of using external nonionizing or acoustic energy to enhance the anti-cancer efficiency of cetuximab. van Driel et al. [28] recently reported of a EGFR targeted nanobody–photosensitizer conjugates for photodynamic therapy in a pre-clinical model of head and neck cancer. These targeted nanobody–conjugates specifically bound to cells over expressing the EGFR and induced phototoxicity. EGFR targeted nanobodies proved to be very selective and potent agents that specifically accumulated in tumours *in vivo* leading to pronounced tumour necrosis. Alternatively, there have been reports that low-intensity US also enhances the anticancer activity of cetuximab in a head and neck cancer cells [29]. Induction of apoptosis was detected by FITC-Annexin V and PI staining assay, 24 hours after cetuximab and/or US treatment. Western blotting analysis of the expression of EGFR, phospho-EGFR, and the upregulated activation of

caspase-3 suggested that US induced the inhibition of EGFR-signaling pathway by cetuximab.

Since the first introduction of applying MBs other than for ultrasound contrast imaging [30], a considerable number of studies have been carried out, evaluating the therapeutic aspects of targeted and non-targeted MBs especially in conjunction with various anticancer drugs. Heath et al. [31] demonstrated increased uptake of fluorescent labeled cetuximab into 4 head and neck carcinoma cell lines in the presence of a non-targeted commercially available lipid based MB contrast agent, Definity®. In vivo tumours treated with cetuximab and adjuvant MB/ultrasound exhibited significant decrease in tumour size at termination compared with cetuximab alone. Non-targeted MB in combination with other anticancer drugs such as cisplatin, melphalan, doxorubicin have been reported to increase effectivity against various cancers [32-34]. A human clinical trial was recently conducted using ultrasound and MBs to enhance gemcitabine treatment of inoperable pancreatic cancer [35]. A commercially available lipid based ultrasound contrast agent, SonoVue® was injected intravenously after a 30 minute gemcitabine administration. The patients were treated with a clinical ultrasound imagining device during bubble administration. According to the survival plot comparing patients treated with ultrasound, MBs, and gemcitabine vs gemcitabine alone, the survival curve indicated that the combined treatment group had nearly twice as high median survival compared to treatment with gemcitabine alone; from a median of 8.9 months to 17.6 months. To improve the targeting function of MBs to cancer, monoclonal antibodies have been linked to the MB shell via protein conjugation for molecular ligands specific to cancer cells. Knowles et al. [36] first investigated MBs with biotinylated shells that were conjugated to anti-EGFR antibody cetuximab for such purposes as differentiating benign from malignant lesions. Significantly improved echogenicity was obtained with this targeted contrast agent for detecting head and neck squamous cell carcinoma in mice. More recently,

the same EGFR targeted MBs were applied to glioma tumour cells in mice and irradiated with therapeutic low intensity pulsed ultrasound [37]. Ultrasound glioma tumour imaging clearly showed accumulation of the targeted MBs as well as significant suppression of tumour growth at 35 days compared to non-targeted MBs.

The present experimental results were in agreement with previously reported targeted MB as to effects on cancer cells only that instead of lipid based shells, our MBs uses human serum albumin. Interestingly, we found that multiple procedures in manufacturing targeted albumin MBs were not necessary compared to lipid based MBs where centrifugal washing, purification, biotin-streptavidin conjugation incubation is essential. Secondly, although lipid based MBs show great possibilities as drug carriers and ultrasound contrast agents, they are occasionally known to induce hypersensitivity reactions that are believed to be associated with complement activation. Furthermore, phospholipids are relatively unstable, being especially susceptible to enzymatic degradation. Liposome based MBs are often expensive due to costs associated with extraction, synthesis and storage (38-40). We believe that our MBs are more advantageous over lipid based MBs from the above reasons but further evaluation is warranted to prove the safety and durability of albumin MBs.

The exact mechanisms by which ultrasound specifically killed HSC-2 cells and induced apoptosis in the presence of targeted MBs are still unknown. In the present study, trypan blue dye method was performed which directly reflects acute cell damage. Microstreaming, microjets, stable and inertial cavitation, are possible candidates that could cause transient or permanent damage to the cell membrane. As is well known, these acoustic phenomena are induced by the oscillations or destructions of MBs activated under acoustic stimulation. We recently reported observation with a high-speed microscopic video of the interaction dynamics between suspended cancer cells and MBs during ultrasound irradiation [17]. It was suggest that the linear oscillation of MB caused microstreaming well below the inertial

cavitation threshold resulting in the deformation of the cell geometry. The shear stress upon the cell membrane could only be achieved when cell and bubble is within a short distance. As sonoporation and gene delivery into cells were demonstrated in this particular study, it is likely that mechanical stress to the cell membrane and underlining cell structure beneath could also initiate apoptosis. Conventional US contrast agents are known to activate caspases, a group of enzymes involved in apoptotic cascade events [41]. Furthermore, previous studies have suggested that the location and the number of MB can determine the degree of damage and repairing of cell membrane [42]. The cell-bubble distance would be a critical factor for defining the shear stress on the cell membrane, hence, our findings of increased cell killing and apoptosis induction by adhering CCAM to cell membrane surface are consistent with this hypothesis. Also the fact that relatively high ratio of the number of sub-micron sized albumin bubbles included in our experiment may have to some extent, altered the efficiency of cell killing and apoptosis. Nevertheless, as the present study is limited to *in vitro* situations, further optimizations of the ultrasound conditions and MB targeting in animal studies are necessary to achieve clinically relevant therapeutic efficacy.

Conclusion

In conclusion, we successfully demonstrated that low intensity US irradiation in conjunction with cetuximab coated albumin MBs selectively killed and induced apoptosis in EGFR- expressing oral squamous cell carcinoma cells. As this MB was easily visualized with conventional ultrasound contrast imaging device, similar albumin based targeting MB agent may become a promising platform for theranostics of various carcinomas.

Acknowledgments

This study was in part supported by Grant-in-Aid for Scientific Research from the Ministry of Education, Culture, Sports, Science and Technology of Japan (# 26670303)

Conflicts of Interest

All the authors of this paper declare that they have no conflicts of interest.

References

1. U. Duvvuri, JN. Myers, Cancer of the head and neck is the sixth most common cancer worldwide. Curr Probl Surg. 2009;46:114-117.
2. C. Scully, J. Bagan, Oral squamous cell carcinoma overview. Oral Oncol. 2009;45:301-308.
3. S. Marur, AA. Forastiere, Head and Neck Squamous Cell Carcinoma: Update on Epidemiology, Diagnosis, and Treatment. Mayo Clin Proc. 2016;91:386-396.
4. JA. Bonner, PM. Harari, J. Giralt, et al. Radiotherapy plus Cetuximab for Squamous-Cell Carcinoma of the Head and Neck. N Engl J Med. 2006;354:567-578.
5. L.A. Torre, F. Bray, R.L. Siegel, et al. Global cancer statistics 2012 CA. Cancer J Clin. 2015;65:87–108
6. D. Shi, L. Guo, S. Duan, et al. Influence of tumor cell lines derived from different tissue on sonoporation efficiency under ultrasound microbubble treatment. Ultrason Sonochem. 2016; DOI:10.1016/j.ultsonch.2016.08.022.
7. Yu FTH, Chen X, Wang J, et al. Low Intensity Ultrasound Mediated Liposomal Doxorubicin Delivery Using Polymer Microbubbles. Mol. Pharm. 2016;13:55‑64.
8. Escoffre JM, Novell A, Serrière S, Lecomte T, Bouakaz A. Irinotecan delivery by microbubble-assisted ultrasound: In vitro validation and a pilot preclinical study. Mol Pharm. 2013 Jul;10(7):2667‑75.
9. B. H. A. Lammertink, C. Bos, R. Deckers, et al. Sonochemotherapy: from bench to bedside. Front Pharmacol. 2015;6:138.
10. Sennoga CA, Kanbar E, Auboire L, Dujardin P-A, Fouan D, Escoffre J-M, et al. Microbubble-mediated ultrasound drug-delivery and therapeutic monitoring. Expert Opin Drug Deliv. 2016;1‑13.
11. J.L. Chena, A.H. Dhanaliwalaa, A.J. Dixona, et al. Synthesis and characterization of transiently stable albumin- coated microbubbles via a flow-focusing microfluidic device. Ultrasound Med Biol. 2014;40:400–409.
12. F. Kratz, Albumin as a drug carrier: Design of prodrugs, drug conjugates and nanoparticles. J Control Release. 2008;132:171–183.
13. J. P. Arnoletti, A. Frolov, M. Eloubeidi, et al. A phase I study evaluating the role of the anti-epidermal growth factor receptor (EGFR) antibody cetuximab as a radiosensitizer

with chemoradiation for locally advanced pancreatic cancer. Cancer Chemother Pharmacol. 2011;67:891–897.

14. J. Baselga, The EGFR as a target for anticancer therapy—focus on cetuximab. Eur J Cancer. 2001;37:16–22.

15. W. Liu, M. Kang, Y. Qin, et al. Apoptosis-inducing effects of cetuximab combined with radiotherapy and hypothermia on human nasopharyngeal carcinoma CNE cells. Int J Clin Exp Med. 2015;8:2182-2189.

16. J.A. Bonner, H.Q. Trummell, A.B. Bonner, et al. Enhancement of Cetuximab-Induced Radiosensitization by JAK-1 Inhibition. BMC Cancer. 2015;15:673.

17. S.M. Nejad, H. Hosseini, H. Akiyama, et al. Reparable Cell Sonoporation in Suspension: Theranostic Potential of Microbubble. Theranostics. 2016;6:446-455.

18. Zeghimi A, Escoffre JM, Bouakaz A. Role of endocytosis in sonoporation-mediated membrane permeabilization and uptake of small molecules: a electron microscopy study. Phys. Biol. 2015;12:66007.

19. A. Bouakaz, A. Zeghimi, A.A. Doinikov, Sonoporation: Concept and Mechanisms. Adv Exp Med Biol. 2016;880:175-189.

20. L.B. Feril Jr, T. Kondo, Q.L. Zhao, et al. Enhancement of ultrasound-induced apoptosis and cell lysis by echo-contrast agents. Ultrasound Med Biol. 2003;29:331-337.

21. Ikeda-Dantsuji Y, Feril LB, Tachibana K, et al. Synergistic effect of ultrasound and antibiotics against Chlamydia trachomatis-infected human epithelial cells in vitro. Ultrason. Sonochem. 2011;18:425‑430.

22. Bruus H. Acoustofluidics 2: Perturbation theory and ultrasound resonance modes. Lab Chip. 2012;12(1):20‑8.

23. A. O. Elzoghby, W. M. Samy, N. A. Elgindy, Albumin-based nanoparticles as potential controlled release drug delivery systems. J Control Release. 2012;157:168–182.

24. Z. Liu, X. Chen, Simple bioconjugate chemistry serves great clinical advances: albumin as a versatile platform for diagnosis and precision therapy. Chem Soc Rev. 2016;45:1432-1456.

25. A.W. Appis, M.J. Tracy, S.B. Feinstein, Update on the safety and efficacy of commercial ultrasound contrast agents in cardiac applications. Echo Res Pract. 2015;2:R55-62.
26. Wu B, Qiao Q, Han X, et al. Targeted nanobubbles in low-frequency ultrasound-mediated gene transfection and growth inhibition of hepatocellular carcinoma cells. Tumor Biol. 2016;37:12113‑12121.
27. J. Baselga, The EGFR as a target for anticancer therapy--focus on cetuximab. Eur J Cancer. 37 Suppl. 2001;4:S16-22.
28. P.B.A.A. van Driel, M.C. Boonstra, M.D. Slooter, et al. EGFR targeted nanobody–photosensitizer conjugates for photodynamic therapy in a pre-clinical model of head and neck cancer. J Control Release. 2016;229:93–105.
29. T. Masui, O. Ichiro, M. Kanno, et al. Low-intensity ultrasound enhances the anticancer activity of cetuximab in human head and neck cancer cells. Exp. Ther. Med. 2013;5:11–16.
30. K. Tachibana, S. Tachibana, Albumin microbubble echo-contrast material as an enhancer for ultrasound accelerated thrombolysis. Circulation. 1995;92:1148–1150.
31. C.H. Heath, A. Sorace, J. Knowles, et al. Microbubble therapy enhances anti-tumor properties of cisplatin and cetuximab in vitro and in vivo. Otolaryngol Head Neck Surg. 2012;146:938–45.
32. B.H.A. Lammertink, C. Bos, K.M. van der Wurff-Jacobs, et al. Increase of intracellular cisplatin levels and radiosensitization by ultrasound in combination with microbubbles. J Control Release. 2016;238:157–165.
33. M. Matsuo, K. Yamaguchi, L.B. Feril, et al. Synergistic inhibition of malignant melanoma proliferation by melphalan combined with ultrasound and microbubbles. Ultrason Sonochem. 2011;18:1218–1224.
34. J.M. Escoffre, J. Piron, A. Novell, et al. Doxorubicin Delivery into Tumour Cells with Ultrasound and Microbubbles. Mol Pharm. 2011;8:799–806.
35. G. Dimcevski, S. Kotopoulis, T. Bjånes, et al.A human clinical trial using ultrasound and microbubbles to enhance gemcitabine treatment of inoperable pancreatic cancer. J Control Release. 2016;243:172–181.
36. J.A. Knowles, C.H. Heath, R. Saini, et al. Molecular targeting of ultrasonographic contrast agent for detection of head and neck squamous cell carcinoma. Arch Otolaryngol Head Neck Surg. 2012;138:662–628.

37. A.-H. Liao, H.-Y. Chou, Y.-L. Hsieh, et al. Enhanced Therapeutic Epidermal Growth Factor Receptor (EGFR) Antibody Delivery via Pulsed Ultrasound with Targeting Microbubbles for Glioma Treatment. J Med Biol Eng. 2015;35:156–164.
38. P.A. Carlson, M.H. Gelb, P. Yager, Zero-order interfacial enzymatic degradation of phospholipid tubules. Biophys J. 1997;73:230–238.
39. G. Bastiat, P. Oliger, G. Karlsson, et al. Development of Non-Phospholipid Liposomes Containing a High Cholesterol Concentration. Langmuir. 2007;23:7695–7699.
40. R.K. Gupta, C.L. Varanelli, P. Griffin, et al. Adjuvant properties of non-phospholipid liposomes (Novasomes) in experimental animals for human vaccine antigens. Vaccine. 1996;14:219–25.
41. L. Zhao, Y. Feng, A. Shi, et al. Apoptosis Induced by Microbubble-Assisted Acoustic Cavitation in K562 Cells: The Predominant Role of the Cyclosporin A-Dependent Mitochondrial Permeability Transition Pore. Ultrasound Med Biol. 2015;41:2755–2764.
42. N. Kudo, K. Okada, K. Yamamoto, Sonoporation by Single-Shot Pulsed Ultrasound with Microbubbles Adjacent to Cells. Biophys J. 2009;96:4866–4876

Legends

Fig. 1. Characterization of CCAM by light scattering measurement system. Size distribution of microbubble diameter (nm).

Fig. 2. Immediate cytotoxicity of cetuximab at various concentrations to (A) HSC-2 cells and (B) U937 cells.

Fig. 3. Comparison of cell survival rate after US irradiation at various intensities. (A) HSC-2 cells and (B) U937 cells. Each data point represents mean ± S.D. (n=4, *p<0.05, ns=not significant).

Fig. 4. Change of percentage of apoptotic cells after US irradiation at an intensity of $0.9W/cm^2$ for 15 sec in the presence of targeted bubble cetuximab (375 μg/mL). Each data point represents mean ± S.D. (n=4, *p<0.05, ns=not significant)).

Fig. 5. Representative bright field and fluorescent microscopic images of HSC-2 cells in the presence of microbubbles. Scale bar in all images are 30μm. (A) Bright field image of HSC-2 cells and microbubbles, (B) fluorescent microscopic image of cells (a), Texas red tagged albumin microbubbles (b), (C) FITC-tagged cetuximab coated microbubbles, (D) merged image of both fluorescent albumin and cetuximab coated microbubbles.

Fig. 6. Comparison of the number of targeted or non-targeted microbubbles adhering to the surface of HSC-cells. Each data point represents mean ± S.D. (n=5, *p<0.05)

Fig. 7. Ultrasound images from the flow model phantom study. Ultrasound images before (A) and after (B) injection of albumin microbubbles into flow vessel (left: standard imaging. right: contrast enhanced imaging). (C) Albumin microbubble time-signal intensity curve in the lumen of flow vessel (the region of interest (ROI), yellow circle area). (D) Cetuximab coated albumin microbubble time-signal intensity curve.

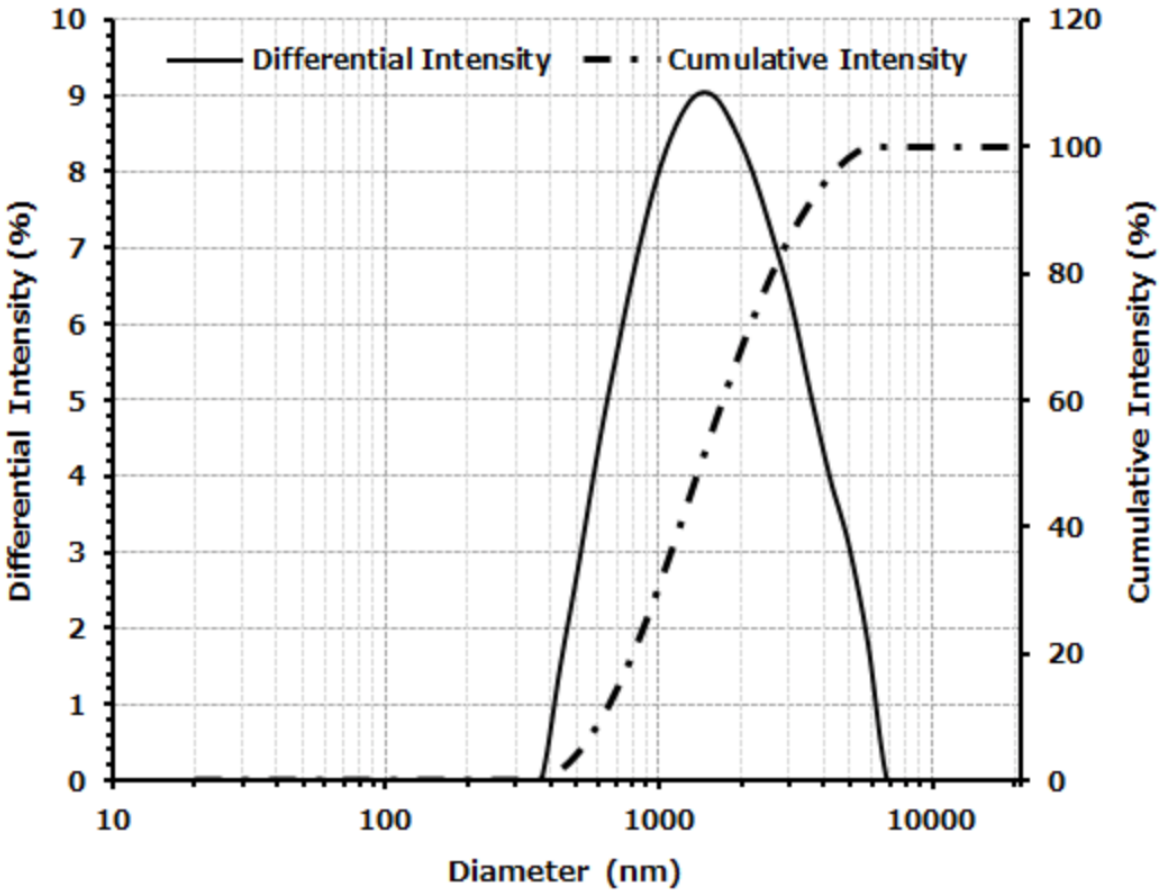
Differential Intensity
Cumulative Intensity
Differential Intensity (%)
Cumulative Intensity (%)
Diameter (nm)
10
100
1000
10000
0
1
2
3
4
5
6
7
8
9
10
0
20
40
60
80
100
120

1

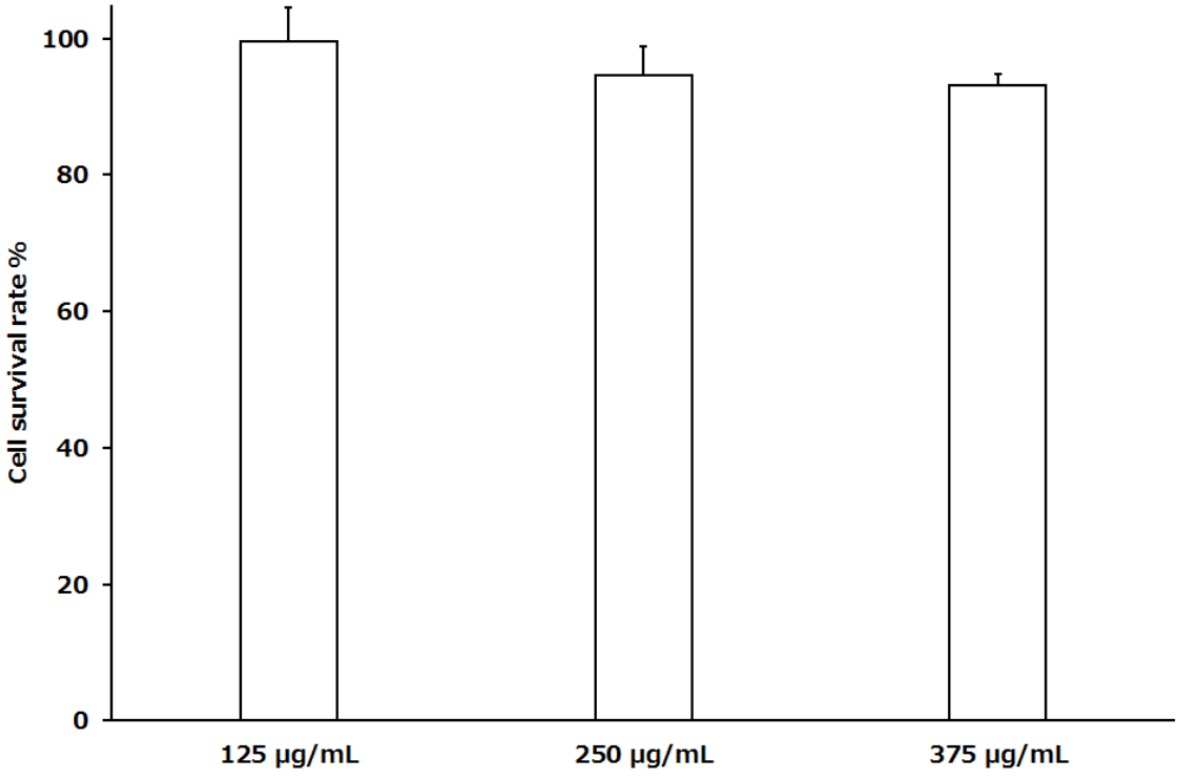
Cell survival rate %
0
20
40
60
80
100
125 μg/mL
250 μg/mL
375 μg/mL

2

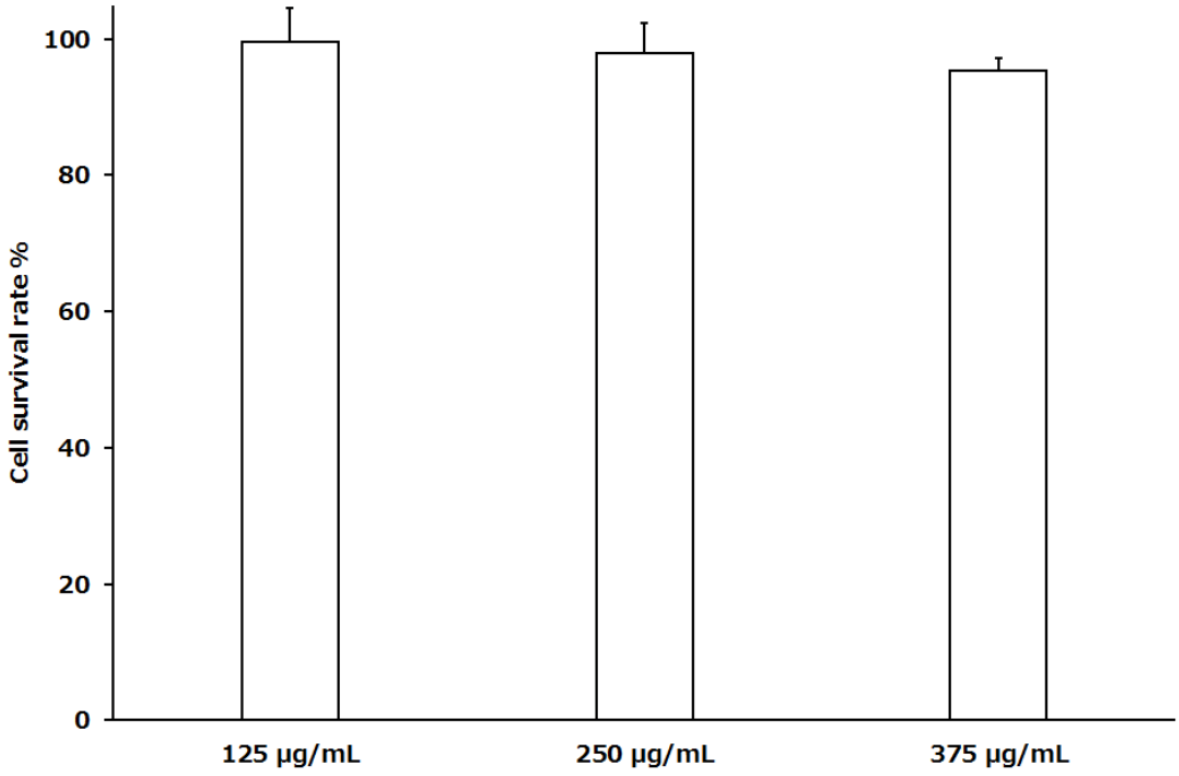
Cell survival rate %
100
80
60
40
20
0
125 μg/mL
250 μg/mL
375 μg/mL

1

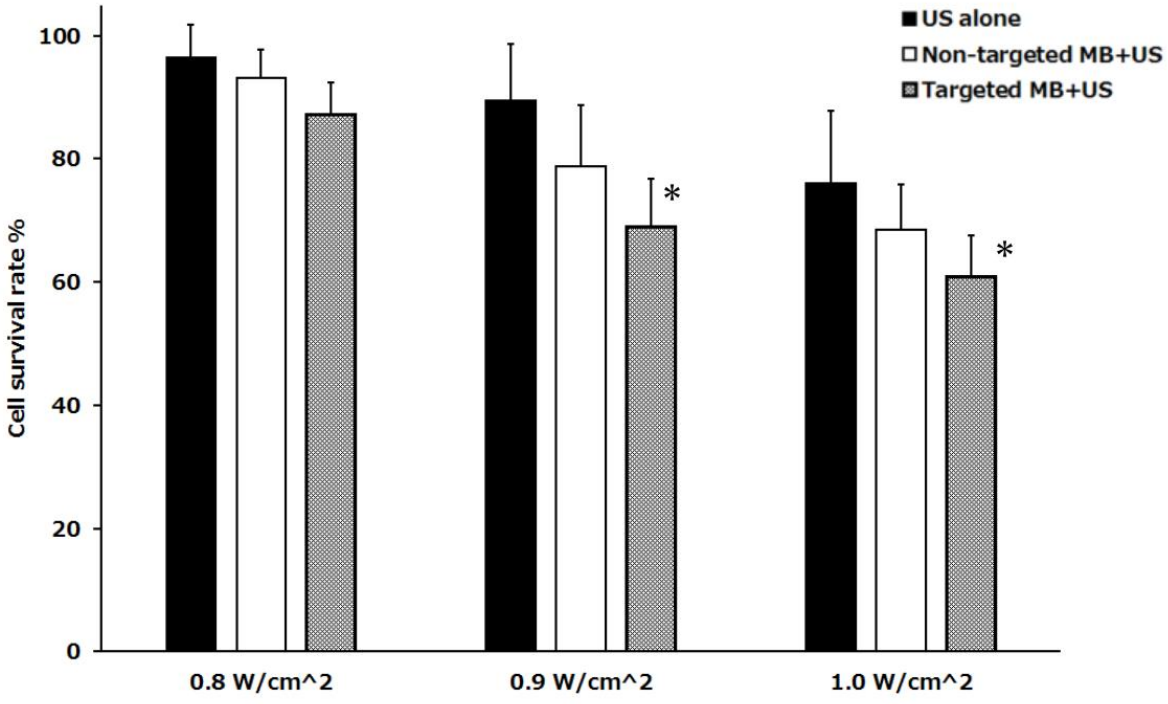
US alone
Non-targeted MB+US
Targeted MB+US
Cell survival rate %
100
80
60
40
20
0
*
*
0.8 W/cm^2
0.9 W/cm^2
1.0 W/cm^2

2

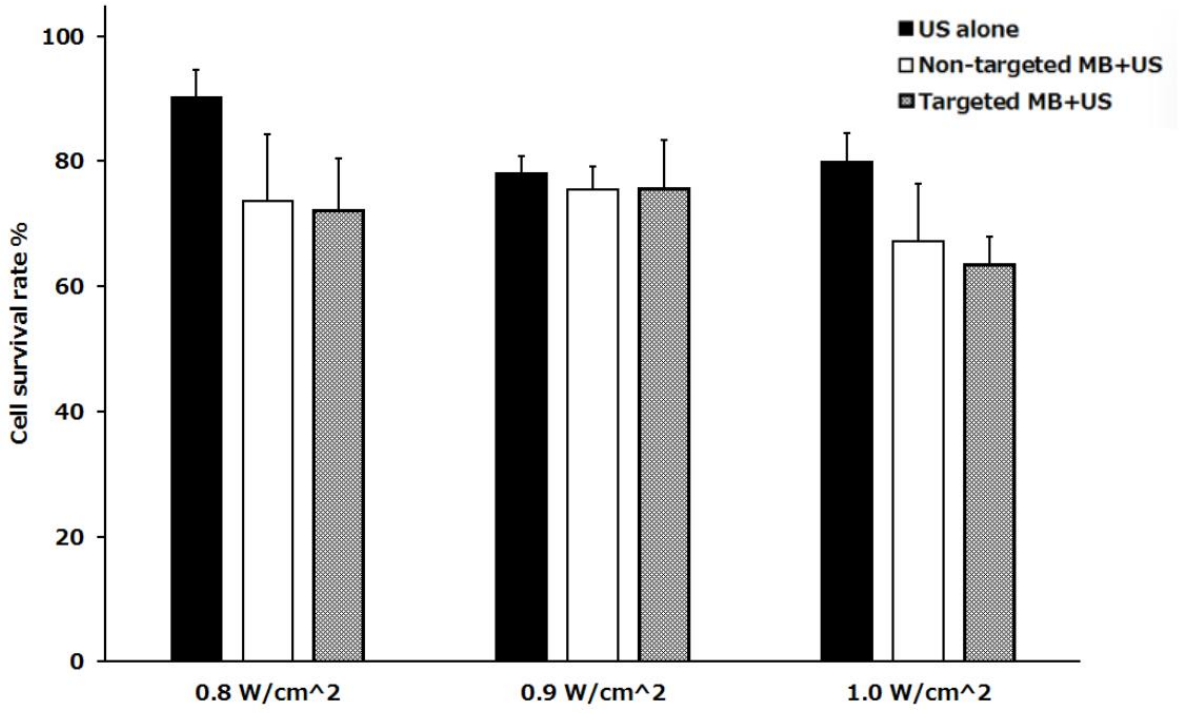
US alone
Non-targeted MB+US
Targeted MB+US
Cell survival rate %
100
80
60
40
20
0
0.8 W/cm^2
0.9 W/cm^2
1.0 W/cm^2

1

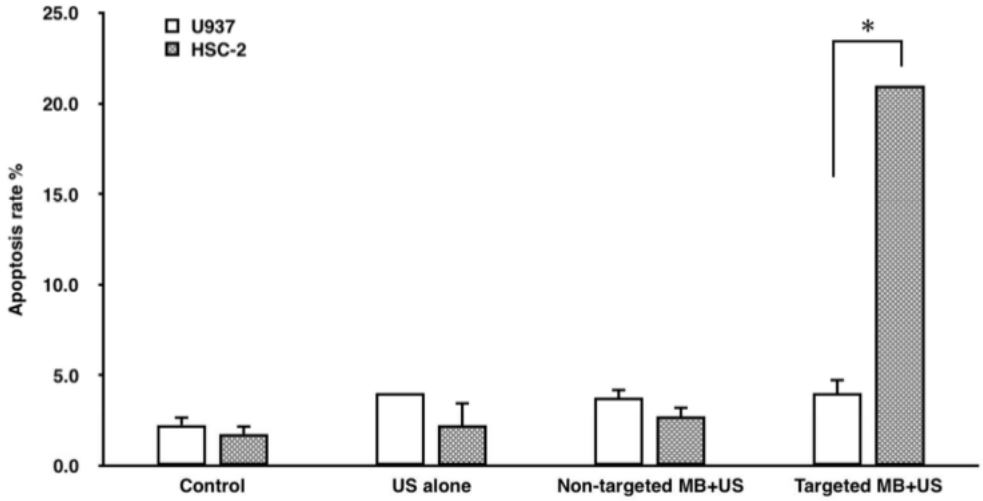
U937
HSC-2
Apoptosis rate %
25.0
20.0
15.0
10.0
5.0
0.0
*
Control
US alone
Non-targeted MB+US
Targeted MB+US

2

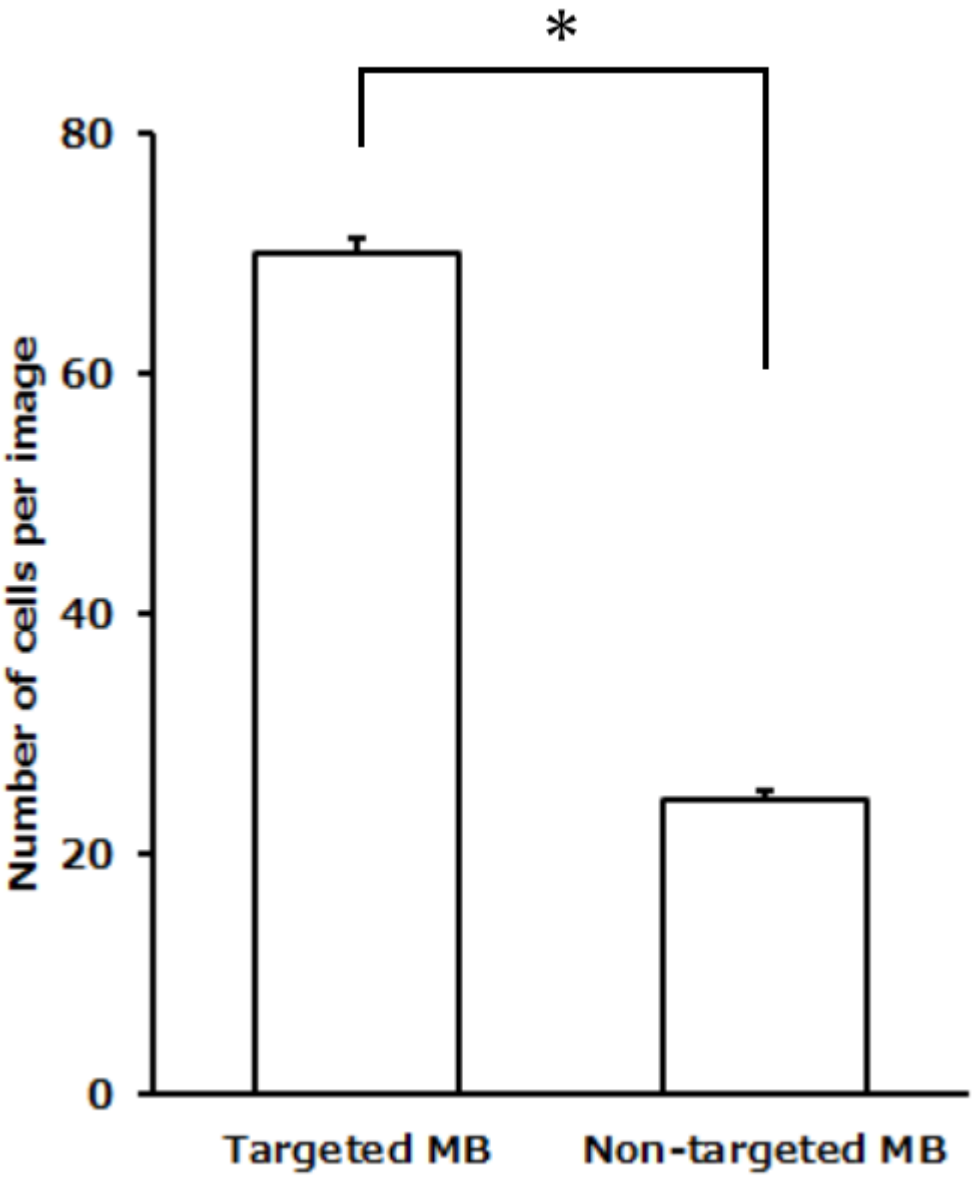
*
80
60
40
20
0
Number of cells per image
Targeted MB
Non-targeted MB

1

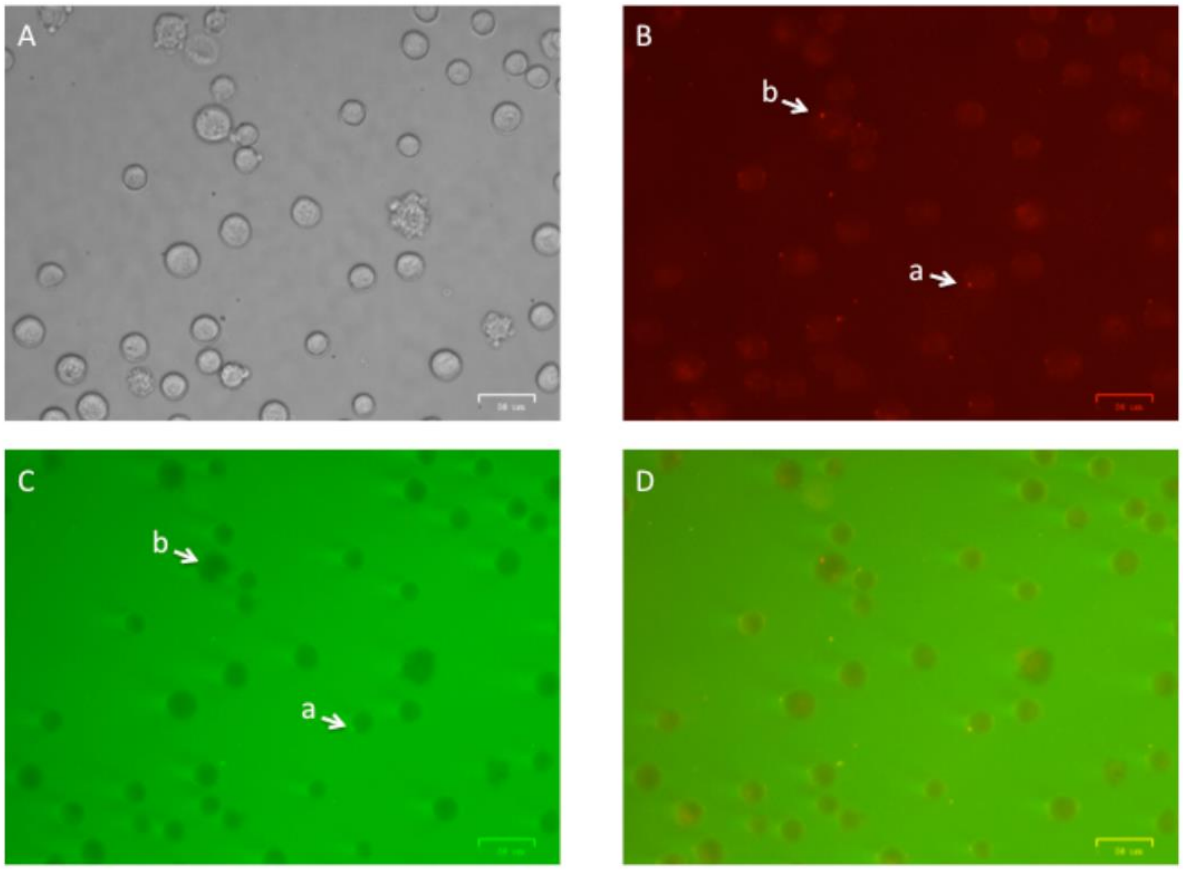

1

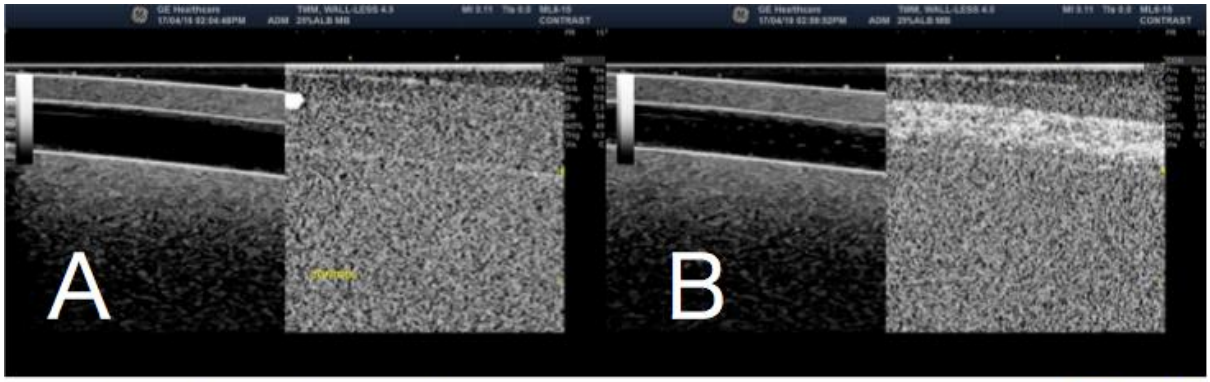
A
B

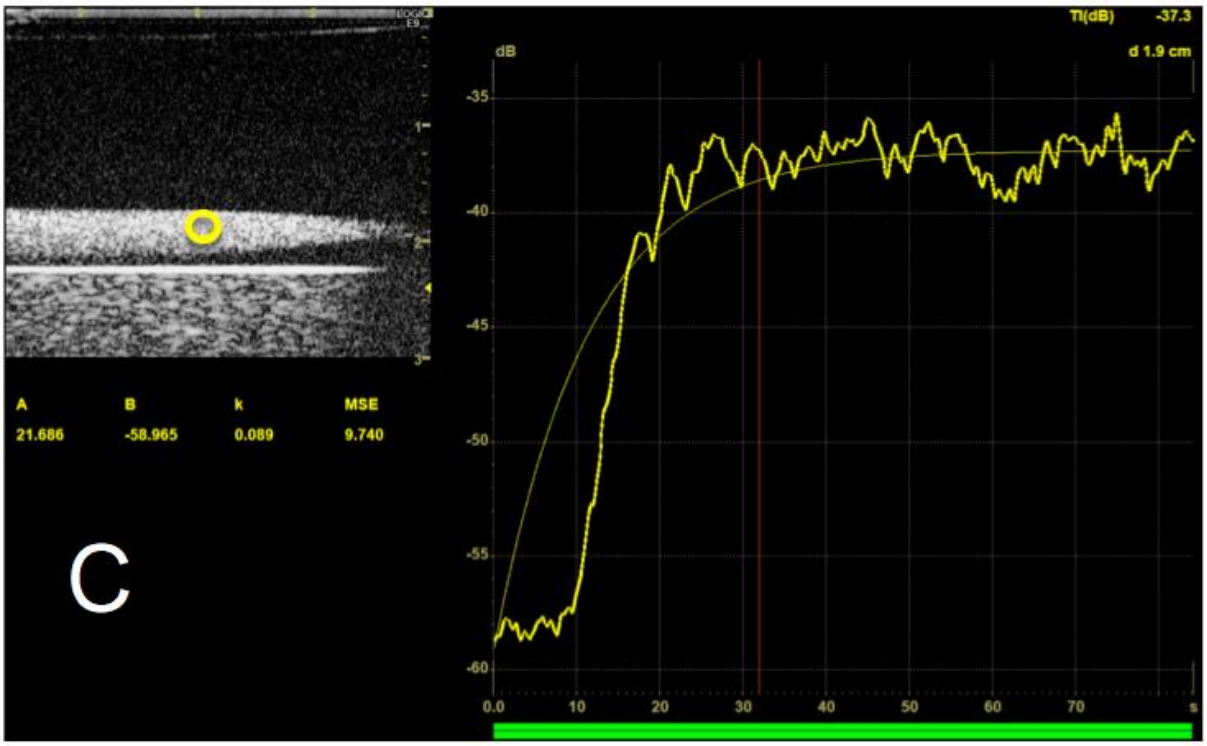
TI(dB) -37.3
d 1.9 cm
dB
-35
-40
-45
-50
-55
-60
0.0
10
20
30
40
50
60
70
s
A B k MSE
21.686 -58.965 0.089 9.740
C

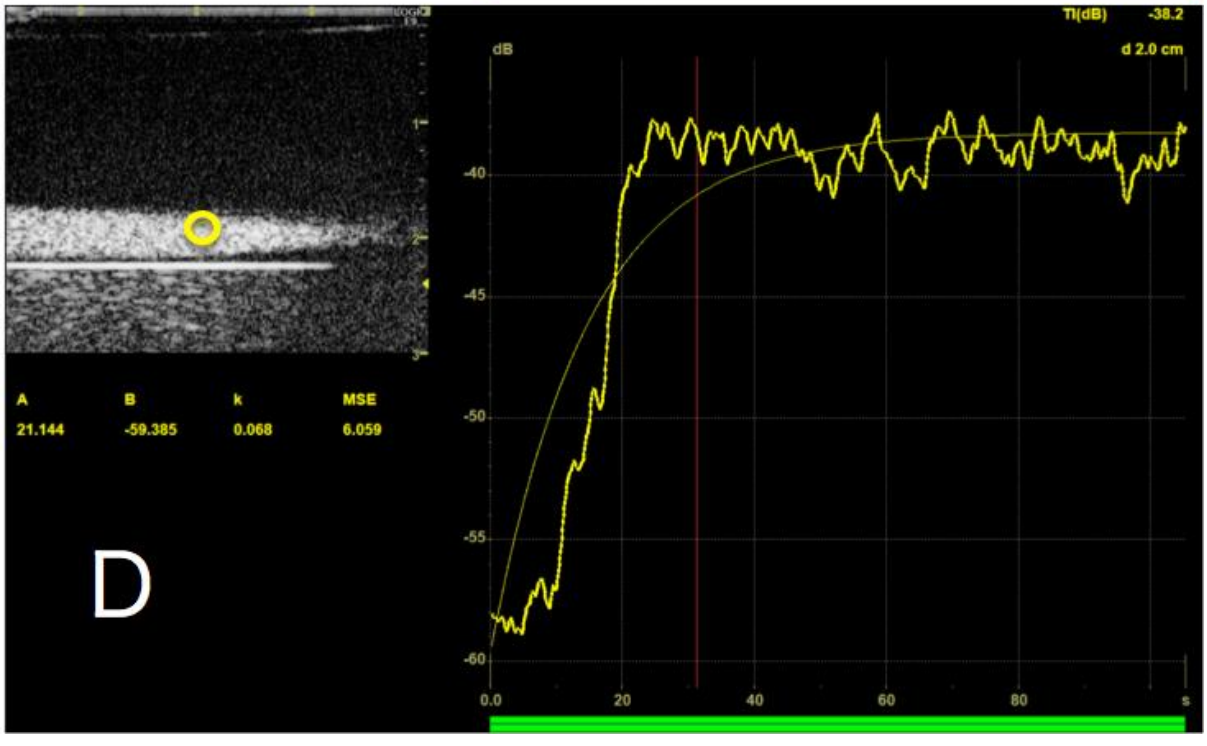
TI(dB) -38.2
d 2.0 cm
dB
-40
-45
-50
-55
-60
0.0
20
40
60
80
s
A B k MSE
21.144 -59.385 0.068 6.059
D

1